Christoph Kern
Andreas Jess*

Design of Unsteady-State Fixed-Bed Processes for Heat Regeneration, Ad-/Desorption, and Gas-Solid Reactions

This review covers all three unsteady-state fixed-bed processes important in chemical engineering, namely, heat transfer from a hot gas to a cold fixed bed (heat regenerator), ad- and desorption of a gas for a Langmuir and a linear isotherm, and regeneration of a coked catalyst by coke burn-off as an important example of a transient gas-solid process. Albeit of inherent differences, the processes have strong analogies. For example, a moving heat or mass transfer zone, spreading or with constant pattern behavior, is formed. For each case, numerical and suitable analytical solutions for process design either selected from literature or developed in this work are derived and compared. Experimental data, if available, are also considered.

1 Introduction

Three important unsteady-state fixed-bed processes are industrially applied and still the subject of intensive research in chemical engineering, particularly 2) and 3):

1) heat transfer from a hot gas to a cold fixed bed (or vice versa) in a heat regenerator,
2) adsorption and desorption of a gas to and from a solid adsorbent, and
3) regeneration of a coked catalyst by coke burn-off, as inspected in this article, but there are similar transient gas-solid processes such as oxidation/reduction of metals/metal oxides or of catalysts with a metal as active component.

The reader may ask, why a review is needed, as these processes are already in industrial operation for many decades and have been also discussed in textbooks and journals, for example, just to name a few, in [1–11] for heat regenerators, in [12–27] for ad-/desorption, and in [12, 28–30] for coke burn-off. The answers to this question and the motivation for this review are:

– The three processes have never been presented and analyzed connectedly in one article in spite of distinct analogies with regard to the transient nature, physicochemical background, and underlying differential equations (DEs).
– Suitable approximate analytical solutions, partly introduced in the literature, although not easy to find, have also not been presented in one article, and were only in parts systematically compared both with numerical solutions and with experimental data.
– The type of the transfer zone formed in each case is often just named as constant pattern or dispersive behavior with-

out a real plausible explanation even for chemical engineers, if not being absolute specialists of one of the named processes. The same is true for methods to calculate the height of the transfer zone (*HTZ*), which is constant or rises in direction of flow.

In this paper, (approximate) analytical and numerical solutions of these three transient fixed-bed systems are reviewed based on literature references and own considerations. The results are compared to experimental literature data, if available. Among other aspects, the type of the moving transfer zone, spreading or with a constant pattern behaviour, is derived. Methods to calculate design parameters, such as the velocity and height of the transfer zone, are given.

2 Heat Transfer from a Hot Gas to a Cold Fixed Bed or Vice Versa (Heat Regenerator)

The heat regenerator was the first unsteady-state fixed-bed process analyzed on a scientific basis. Already in the 1920s, Anzelius, Nusselt, and Hausen made significant contributions to mathematical design methods [1, 2, 8]. The process requires a two-step operation. In the first step a hot gas gives up its heat to a cold fixed bed. The bed heats up and in the second step

Dr. Christoph Kern, Prof. Dr. Andreas Jess
jess@uni-bayreuth.de
Chair of Chemical Engineering, Center of Energy Technology, University of Bayreuth, Universitätsstr. 30, 95440 Bayreuth, Germany.

releases the heat to a second cold gas. For continuous operation regenerators are used in pairs.

A prominent example is preheating of air blown into blast furnaces, where inlet temperatures of 1300 °C are needed, too hot for construction materials of recuperators (stationary operated and much easier to design). Hence, regenerators (cowper stoves) are needed. The heating of the typically used checker bricks is conducted by hot flue gas generated in an upstream combustion chamber by incineration of the waste gas of the blast furnace. During the subsequent discharge period, fresh air is driven across the hot bricks. Other regenerator applications are glassmaking furnaces or coal power stations, if dirty or dust-laden gases are liable to plug recuperators [4].

On first sight, the regenerator seems to be simple, as only heat exchange is involved without any change of the composition of solid and fluid. But as Jakob stated in 1957, "the theories of the regenerator are among the most difficult and involved that are encountered in engineering" [3]. This statement is still valid, even if numerical solutions of the DEs, also presented in this work, are today relatively simple to achieve by computer programs. But the results of mere numerical calculations always have in general one crucial drawback: You have to trust the results, even if not immediately clear, e.g., here the influence of the operation time or of the axial position on the shape and width of the moving transfer zone, a characteristic feature of every transient fixed-bed process. Additional analytical (approximate) solutions are therefore still of high value with regard to a process understanding and to check numerically derived results.

According to Levenspiel [4, 5], the spreading of the temperature front in a regenerator and thus the HTZ are determined by three phenomena: 1) gas-solid heat transfer, 2) axial dispersion of heat by the gas and solid, often collectively described by an effective axial thermal conductivity, and 3) conductive heat flow into the particles. Dispersion is only important for strong T-variations over a length of a few particles. Spreading by heat conduction into the particles only comes into play, if the time for particle heating is comparatively large (low thermal conductivity of solid). Here, it is assumed that the spreading of the T-front, as in most technical cases, is only governed by the external gas-solid heat transfer. The differential equations for a regenerator are then:

$$\varepsilon_{\text{bed}} \frac{\partial T_{\text{g}}}{\partial t} + u_{\text{s}} \frac{\partial T_{\text{g}}}{\partial z} = -\frac{\rho_{\text{bed}} \, c_{\text{s,m}}}{\rho_{\text{g,mol}} \, c_{\text{p,g,mol}}} \frac{\partial T_{\text{s}}}{\partial t} \qquad (1)$$

$$\frac{\partial T_{\text{s}}}{\partial t} = \frac{\alpha_{\text{ex}} \, a_{\text{V}} \left(T_{\text{g}} - T_{\text{s}}\right)}{\rho_{\text{bed}} \, c_{\text{s,m}}} \quad \text{with } a_{\text{V}} = \frac{6(1-\varepsilon_{\text{bed}})}{d_{\text{p}}} \text{ for spherical particles} \qquad (2)$$

The Eqs. (1) and (2) lead to

$$\varepsilon_{\text{bed}} \frac{\partial T_{\text{g}}}{\partial t} + u_{\text{s}} \frac{\partial T_{\text{g}}}{\partial z} = \frac{\alpha_{\text{ex}} \, a_{\text{V}}}{\rho_{\text{g,mol}} \, c_{\text{p,g,mol}}} \left(T_{\text{s}} - T_{\text{g}}\right) \qquad (3)$$

Typically, the boundary and initial conditions are a constant gas inlet temperature $(T_{\text{g,in}})$[1] and a uniform initial solid temperature $(T_{\text{s,0}})$. Eq. (3) is also useful to calculate the gas-solid temperature difference, if $\partial T_{\text{g}}/\partial z$ is known and the condition

$\varepsilon_{\text{bed}} \, \partial T_{\text{g}}/\partial t \ll u_{\text{s}} \partial T_{\text{g}}/\partial z$ is fulfilled, as validated below. The condition $\left| T_{\text{g}} - T_{\text{g,in}} \right| = 0.5 \left| T_{\text{g,in}} - T_{\text{s,0}} \right| = 0.5 \left| \Delta T_{\text{g,max}} \right|$ is then typically used as reference with the corresponding position $z_{0.5}$ and time $t_{0.5}$, respectively:

$$\left(T_{\text{g}} - T_{\text{s}}\right)_{0.5} \approx -\frac{u_{\text{s}} \, \rho_{\text{g,mol}} \, c_{\text{p,g,mol}}}{\alpha_{\text{ex}} \, a_{\text{V}}} \left(\frac{\partial T_{\text{g}}}{\partial z}\right)_{0.5} \quad \text{for} \quad \varepsilon_{\text{bed}} \frac{\partial T_{\text{g}}}{\partial t} \ll u_{\text{s}} \frac{\partial T_{\text{g}}}{\partial z} \qquad (4)$$

According to Levenspiel [4, 5], the symmetrical S-shaped advancing temperature front is well represented by the Gaussian cumulative distribution function (CDF) with standard deviation σ_{T}:

$$\sigma_{\text{T}} = t \sqrt{\frac{2 \, u_{\text{s}}}{z} \frac{\rho_{\text{g,mol}} \, c_{\text{p,g,mol}}}{\alpha_{\text{ex}} \, a_{\text{V}}}} \qquad (5)$$

The CDF equation of the T-front, Eq. (S1), useful approximate solutions, Eqs. (S2) and (S3), and also a method to determine the HTZ are given in the Supporting Information (Sect. S1).

Symmetrical S-shaped fronts of T_{g} and T_{s} only develop, i.e., Eqs. (5) and (S1) are valid, if the spreading of the front is caused by only one phenomenon, here, as stated before, only by gas-solid heat transfer. The validity of this assumption in general and for the example given below is elucidated in Sect. S2. Secondly, the regenerator should be so long that the particles at the inlet of the bed almost reach $T_{\text{g,in}}$, at least for most of the regenerator's operation time.

The velocity of the front determines the time $t_{0.5}$ the center of the in the ideal case symmetrical S-shaped T-profile ($\Delta T_{\text{g,center}} = 0.5 \Delta T_{\text{g,max}}$) needs to reach the axial position $z_{0.5}$:

$$u_{\text{F}} = \frac{z_{0.5}}{t_{0.5}} = u_{\text{s}} \frac{\rho_{\text{g,mol}} \, c_{\text{p,g,mol}}}{\left(\varepsilon_{\text{bed}} \rho_{\text{g,mol}} \, c_{\text{p,g,mol}} + \rho_{\text{bed}} \, c_{\text{s,m}}\right)} \approx u_{\text{s}} \frac{\rho_{\text{g,mol}} \, c_{\text{p,g,mol}}}{\rho_{\text{bed}} \, c_{\text{s,m}}} \qquad (6)$$

Note that u_{F} is independent of temperature ($u_{\text{s}} \sim T$; $\rho_{\text{g,mol}} \sim 1/T$). Combining Eqs. (5) and (6) yields:

$$\sigma_{\text{T}} = t_{0.5} \sqrt{\frac{2 \, u_{\text{F}}}{z_{0.5}} \frac{\rho_{\text{bed}} \, c_{\text{s,m}}}{\alpha_{\text{ex}} \, a_{\text{V}}}} = \frac{z_{0.5}}{u_{\text{F}}} \sqrt{\frac{2 \, u_{\text{F}}}{z_{0.5}} \frac{\rho_{\text{bed}} \, c_{\text{s,m}}}{\alpha_{\text{ex}} \, a_{\text{V}}}} = \sqrt{\frac{2 \, z_{0.5}}{u_{\text{F}}} \frac{\rho_{\text{bed}} \, c_{\text{s,m}}}{\alpha_{\text{ex}} \, a_{\text{V}}}} \sim \sqrt{\frac{z_{0.5}}{u_{\text{F}}}} \qquad (7)$$

For the heating of an initially uniformly cold fixed bed with hot gas, the slope of T_{g} with t at position $z_{0.5}$ or the slope with regard to z at time $t_{0.5}$ is [4, 5]:

$$-\left(\frac{\partial T_{\text{g}}}{\partial t}\right)_{0.5} \approx \frac{T_{\text{g,max}}}{2.5 \, \sigma_{\text{T}}} = \frac{T_{\text{g,max}}}{2.5 \sqrt{2}} \sqrt{\frac{u_{\text{F}} \, \alpha_{\text{ex}} \, a_{\text{V}}}{\rho_{\text{bed}} \, c_{\text{s,m}}}} \sqrt{\frac{1}{z_{0.5}}} \qquad (8)$$

$$-\left(\frac{\partial T_{\text{g}}}{\partial z}\right)_{0.5} \approx \frac{T_{\text{g,max}}}{2.5 \, \sigma_{\text{T}} \, u_{\text{F}}} = \frac{T_{\text{g,max}}}{2.5 \sqrt{2}} \sqrt{\frac{\alpha_{\text{ex}} \, a_{\text{V}}}{u_{\text{F}} \, \rho_{\text{bed}} \, c_{\text{s,m}}}} \sqrt{\frac{1}{z_{0.5}}} \qquad (9)$$

---

[1] List of symbols at the end of the paper.

Hence, the *HTZ*, which is proportional to $1/(\partial T_g/\partial z)$ and thus proportional to $\sqrt{z_{0.5}}$, see Eq. (9), broadens with increasing axial position z and adsorber length, respectively. Note that the *HTZ* is not strictly defined, because it is difficult to determine where the transfer zone begins and ends. Typically the distance of two positions is used, where a certain initial and final *T*-value is reached, for example $z_{0.02}$ is related to $\Delta T_g = 0.02\Delta T_{g,\text{max}}$ and $z_{0.98}$ to $\Delta T_g = 0.98\Delta T_{g,\text{max}}$, and thus the $HTZ = z_{0.98} - z_{0.02}$. Eqs. (8) and (9) also yield the ratio of $\varepsilon_{\text{bed}}\partial T_g/\partial t$ and $u_s\partial T_g/\partial z$, helpful, as already indicated before, to prove the validity of Eq. (4):

$$\frac{\varepsilon_{\text{bed}}\left(\frac{\partial T_g}{\partial t}\right)_{0.5}}{u_s\left(\frac{\partial T_g}{\partial z}\right)_{0.5}} \approx \frac{\varepsilon_{\text{bed}}}{u_s}u_F \tag{10}$$

The front velocity (u_F) is in general much smaller than the gas velocity (u_s), justifying that Eq. (4) is suitable to calculate the difference between T_g and T_s by the quasi-steady-state assumption. For example, $\varepsilon_{\text{bed}}\partial T_g/\partial t/(u_s\partial T_g/\partial z)$ is 0.0002 for the case examined here (parameters in Tab. 1).

The results of the numerical and analytical calculations presented in the Figs. 1 and 2 were validated by experimental data of Uniyal and Sharma for heating of an initially cold fixed bed of rocks with hot air [7] (Fig. 1). For the numerical analysis, Eqs. (1)–(3), as all DEs in this work, were solved by the computer program Presto, a solver of DEs (CiT GmbH, Rastede, Germany). For the analytical solution, the gradient $(dT_g/dz)_{0.5}$ at a certain axial position $z_{0.5}$ is calculated by Eq. (9), and the corresponding symmetrical S-shaped curves by the Gaussian CDF by Eq. (S1), see Supporting Information, with σ_T as standard deviation, Eq. (5). Parameters values and boundary conditions such as the constant value of $T_{g,\text{in}}$ are listed in Tab. 1.

The numerical and analytical solutions almost coincide except for the front section of the bed (< 0.1 m) and operation times < 20 min, Fig. 2. The analytical solution, assuming a symmetrical S-shaped *T*-front, then leads to physically unsensical gas temperatures below $T_{g,\text{in}}$ (Fig. 1), and the solid particles at the inlet of the fixed bed have, according to the numerical analysis, still not reached $T_{g,\text{in}}$ (Fig. 2). The (absolute) value of the *T*-gradient decreases with time and position ($\sim 1/\sqrt{z_{0.5}}$ and $\sim 1/\sqrt{t_{0.5}}$, Fig. 1): The gradient is $-1100\,\text{K m}^{-1}$ for $z_{0.5} = 0.35$ m (50 min) and $-870\,\text{K m}^{-1}$ for 0.56 m (80 min), as postulated by Eq. (9). Hence, the *HTZ* increases proportionally to $\sqrt{z}$.
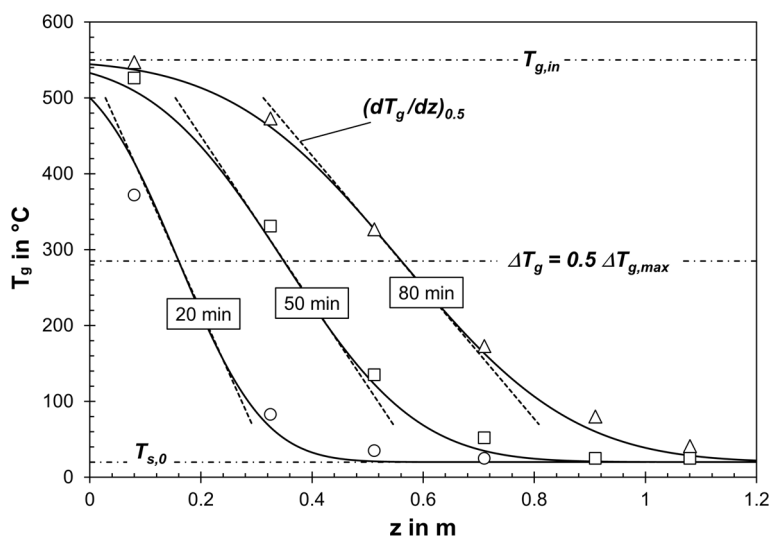
For a reliable applicability of the CDF for a heat regenerator the term σ_T/t should be < 0.4 [4, 5]; one may call this a long regenerator in line with Levenspiel's definition. Here this limit is reached at $z_{0.5} = 0.65$ m after 80 min. Thus, the nevertheless instructive experiments of Uniyal and Sharma [9] were conducted in a still rather short regenerator.

An attempt for a plausible explanation of the spreading phenomenon in a heat regenerator by a simple schematic diagram is shown in Fig. 3 with T_g and T_s in dimensionless terms (Θ_g, Θ_s). The regeneration is regarded as a perpetually repeating two-step process: In a first step (1a), the *T*-profile of the gas (initially a flat front) migrates into the bed by a small axial distance, leading to a shift (offset) from the profile of the solid. This step accounts for the *T*-difference between gas and solid and thus for the gas-solid heat transfer resistance. In a second step (1b), thermal equilibrium is established, here for illustration assuming that the decrease of T_g equals the corresponding rise of T_s ($\Delta T_g = -\Delta T_s$). This two-step process is then repeated (2a/2b–4a/b). Fig. 3 illustrates that in each step the *HTZ* is broadening, and the *T*-gradient $|\partial T_i/\partial z|$ decreases.

Table 1. Model parameters of thermal regenerator (hot air, initially cold rock bed; data from [9]).

Parameter	Value	Unit
$T_{g,\text{in}}$, $T_{s,0}$	550, 20	°C
$\rho_{g,\text{mol},293\,K}$	41	mol m^{-3}
$c_{P,g}$	30	$\text{J mol}^{-1}\text{K}^{-1}$
ρ_{bed}	1978	kg m^{-3}
ε_{bed}	0.4	–
$c_{s,m}$	1068	$\text{J kg}^{-1}\text{K}^{-1}$
α_{ex}	24.5	$\text{W m}^{-2}\text{K}^{-1}$
d_P	0.02	m
a_V	180	m^2m^{-3}
$u_{s,293\,K}$	0.195	m s^{-1}
u_F	0.00011	m s^{-1}
L	1.2	m
p	1	bar

Figure 1. Axial profiles of T_g for heating of a cold rock bed with hot air calculated by Eqs. (5), (9), (S1) and (S2); conditions and parameters in Tab. 1; symbols: measured data [9]). The symmetrical S-shaped T-fronts represent Gaussian CDFs.
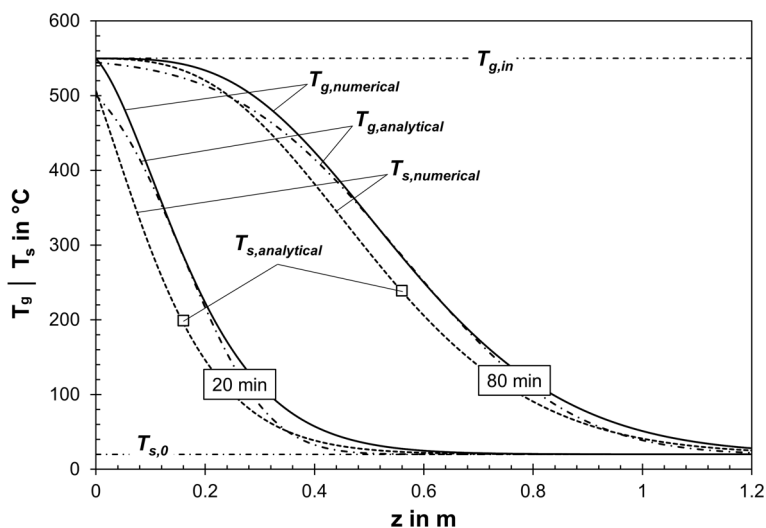
Figure 2. Numerically modeled axial T-profiles based on Eqs. (1) and (2) (solid line for gas and dotted line for solid) and analytical solution for T_g by Eqs. (5), (9), (S1), and (S2) (dashed-dotted line). The two circles show T_s calculated by Eq. (4) for $\Delta T_g = 0.5\,\Delta T_{g,max}$.

3 Ad- and Desorption for a Langmuir Adsorption Isotherm

The equations for ad- and desorption according to the linear driving force model are:

$$\varepsilon_{bed}\frac{\partial c_g}{\partial t} + u_s\frac{\partial c_g}{\partial z} = -\rho_{bed}\frac{\partial \bar{L}_{mol,m}}{\partial t} \tag{11}$$

$$\frac{\partial \bar{L}_{mol,m}}{\partial t} = k_{LDF}\left(L^*_{mol,m} - \bar{L}_{mol,m}\right) \tag{12}$$

Here (and also in Sect. 4), only isothermal ad- and desorption of a single gaseous component is considered. For a Langmuir adsorption isotherm, the equilibrium loading of the adsorbent is:

$$L^*_{mol,m} = \frac{k_{ad,L}\,c_g}{1 + K_{ad,L}\,c_g} \tag{13}$$

$$\bar{L}_{mol,m} = \frac{k_{ad,L}\,\bar{c}_{g,pore}}{1 + K_{ad,L}\,\bar{c}_{g,pore}} \tag{14}$$
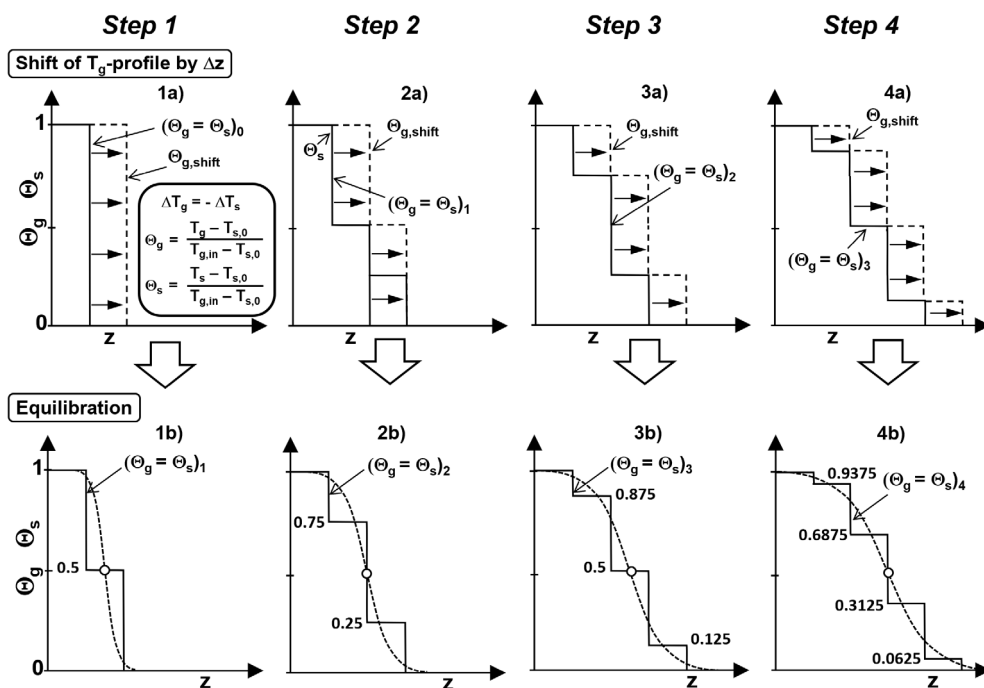
Figure 3. Explanation of spreading phenomenon in a heat regenerator (hot gas/cold bed) by a schematic diagram. The heat transfer process is regarded as a perpetually repeating two-step process (step 1 a: shift (offset) between profiles of T_g and T_s; step 1b: thermal equilibrium assuming $|\Delta T_g| = |\Delta T_s|$). The two-step process is then repeated (2a/2b–4a/4b).

$L^*_{\text{mol,m}}$ and $\bar{L}_{\text{mol,m}}$ are the equilibrium loadings of the adsorbent for the concentration of the adsorbed gas in the bulk phase (c_{g}) and for the mean value in the porous particles ($\bar{c}_{\text{g,pore}}$).

A helpful (but not well-known, as not published in a chemical engineering journal) approximation of the adsorption front equation for a Langmuir isotherm is given by Grevillot [22]:

$$\frac{1}{(1-R)} \ln\left\{ \left(1 - \frac{c_{\text{g}}}{c_{\text{g,in}}}\right) \left(\frac{c_{\text{g,in}}}{c_{\text{g}}}\right)^R \right\} + 1 = k_{\text{LDF}}\left(\frac{z}{u_{\text{F}}} - t\right) \quad \text{for} \quad R < 1 \tag{15}$$

$$R = \frac{1}{1 + K_{\text{ad,L}}\, c_{\text{gas,in}}} \tag{16}$$

$$u_{\text{F}} \approx u_{\text{s}}\frac{c_{\text{g,in}}}{\rho_{\text{bed}}\, L_{\text{mol,m,max}}} = u_{\text{s}}\frac{c_{\text{g,in}}\left(1 + K_{\text{ad,L}}\, c_{\text{g,in}}\right)}{\rho_{\text{bed}}\, L_{\text{mol,m,max}}\, k_{\text{ad,L}}\, c_{\text{g,in}}} \tag{17}$$

The velocity of the adsorption front u_{F} increases proportionally for a rise of the gas velocity u_{s}, reducing the operation time of the adsorber ($t_{\text{breakthrough}}$). Eq. (15) can also be used to determine the *HTZ* of adsorption, see Sect. S3 (Eq. (S14)) of Supporting Information.

The difference in time to reach $0.5c_{\text{g,in}}$ and $0.49c_{\text{g,in}}$, respectively, can be calculated by Eq. (15):

$$t_{0.5} - t_{0.49} = \frac{1}{(R-1)k_{\text{LDF}}}\left[\ln\left(\frac{0.5}{(0.5)^R}\right) - \ln\left(\frac{0.51}{(0.49)^R}\right)\right] \tag{18}$$

Eq. (18) then leads to the constant slope with time or location at $c_{\text{g}} = 0.5c_{\text{g,in}}$ (center of front):

$$\left(\frac{\partial\left(\frac{c_{\text{g}}}{c_{\text{g,in}}}\right)}{\partial t}\right)_{0.5} = -u_{\text{F}}\left(\frac{\partial\left(\frac{c_{\text{g}}}{c_{\text{g,in}}}\right)}{\partial z}\right)_{0.5} \tag{19}$$

$$\approx \frac{0.01}{(t_{0.5} - t_{0.49})} = \frac{(1-R)k_{\text{LDF}}}{(1.98 + 2.02\, R)}$$

A Langmuir isotherm is favorable for adsorption (constant pattern) but unfavorable for desorption (spreading transfer zone). An approximate solution for the desorption profile for an initially uniformly saturated bed ($L_{\text{mol,m,0}}, c_{\text{g,0}}$) was published by Ruthven [17]:

$$\frac{c_{\text{g}}}{c_{\text{g,0}}} = \frac{R}{(1-R)}\left\{\sqrt{\frac{\rho_{\text{bed}}\, k_{\text{ad,L}}\, z}{u_{\text{s}}(t - \tau_{\text{g}})}} - 1\right\} \quad \text{for} \quad \frac{1}{R^2} > \frac{\rho_{\text{bed}}\, k_{\text{ad,L}}}{u_{\text{s}}}\frac{z}{t} > 1$$

$$\text{with} \quad \tau_{\text{g}} = \frac{\varepsilon_{\text{bed}}\, z}{u_{\text{s}}} \tag{20}$$

Rearranging Eq. (20) gives the time $t_{0.5}$ and the local position $z_{0.5}$, respectively:

$$t_{0.5} = \frac{\rho_{\text{bed}}\, k_{\text{ad,L}}\, z_{0.5}}{u_{\text{s}}}\left\{\frac{2R}{(1+R)}\right\}^2 + \tau_g \tag{21}$$

$$z_{0.5} = \left\{\frac{(1+R)}{2R}\right\}^2 \frac{u_{\text{s}}(t_{0.5} - \tau_{\text{g}})}{\rho_{\text{bed}}\, k_{\text{ad,L}}} \tag{22}$$

Derivation of Eq. (20) over time and insertion of Eq. (21) yields the slope of the desorption front with respect to time at $c_{\text{g}} = 0.5c_{\text{g,0}}$, which changes with axial position proportionally to $1/z_{0.5}$:

$$\left(\frac{\partial\left(\frac{c_{\text{g}}}{c_{\text{g,0}}}\right)}{\partial t}\right)_{0.5} = -\frac{(1+R)^3}{16\, R^2(1-R)}\frac{u_{\text{s}}}{\rho_{\text{bed}}\, k_{\text{ad,L}}\, z_{0.5}} \tag{23}$$

Derivation of Eq. (20) with respect to axial position z and insertion of Eq. (22) leads to the slope of the desorption front with regard to z at $c_{\text{g}} = 0.5c_{\text{g,0}}$:

$$\left(\frac{\partial\left(\frac{c_{\text{g}}}{c_{\text{g,0}}}\right)}{\partial z}\right)_{0.5} = \frac{R^2}{(1-R^2)}\frac{\rho_{\text{bed}}\, k_{\text{ad,L}}}{u_{\text{s}}(t_{0.5} - \tau_{\text{g}})} \tag{24}$$

Eq. (20) can also be used to estimate the *HTZ* of desorption, see Sect. S3 (Eq. (S15)).

Subsequently, the solutions by the presented approximate analytical equations are compared to ("correct") numerical solutions. Experimental data of Hwang and Lee [24] for sorption of CO_2 on activated carbon are also presented. The Langmuir isotherm is displayed in Fig. 4. The parameters and the boundary conditions needed to model the sorption are listed in Tab. 2.

The result of the numerical solution of Eqs. (11)–(13) and the analytical results are shown in Fig. 5. At first, a constant value of k_{LDF} was used, determined in [26] by the best match of modelling and experimental data. For comparison, a correlation considering that $k_{\text{LDF,L}}$ depends on the slope of the Langmuir isotherm [12, 19, 20, 25], was also used:

$$k_{\text{LDF,L}} = \frac{60}{d_{\text{p}}^2}D_{\text{eff,ad}} = \frac{60\, D_{\text{eff,pore}}}{d_{\text{p}}^2\left(\varepsilon_{\text{p}} + \rho_{\text{p}}\frac{dL_{\text{mol,m}}}{dc_{\text{g}}}\right)}$$

$$= \frac{60\, D_{\text{eff,pore}}}{d_{\text{p}}^2}\left(\varepsilon_{\text{p}} + \rho_{\text{p}}\frac{k_{\text{ad,L}}}{(1 + K_{\text{ad,L}}\, c_{\text{g}})^2}\right)^{-1} \tag{25}$$

$D_{\text{eff,ad}}$ is an apparent diffusion coefficient considering that the adsorption equilibrium affects the adsorption rate. The effective pore diffusion coefficient $D_{\text{eff,pore}}$ is given by:

$$D_{\text{eff,pore}} \approx \frac{\varepsilon_{\text{p}}}{\tau_{\text{p}}}D_{\text{pore}} = \frac{\varepsilon_{\text{p}}}{\tau_{\text{p}}}\left(\frac{1}{D_{\text{mol}}} + \frac{1}{D_{\text{Kn}}}\right)^{-1} \tag{26}$$

The numerical and analytic solution of CO_2 adsorption (Langmuir isotherm; constant k_{LDF}) are in perfect agreement and also reflect the measured breakthrough curve for a bed length of 0.5 m well (Fig. 5). Comparison with the c_{CO_2} curve for a length of 1 m indicates the expected constant pattern behavior. Complementary, c_{CO_2} profiles versus distance z for
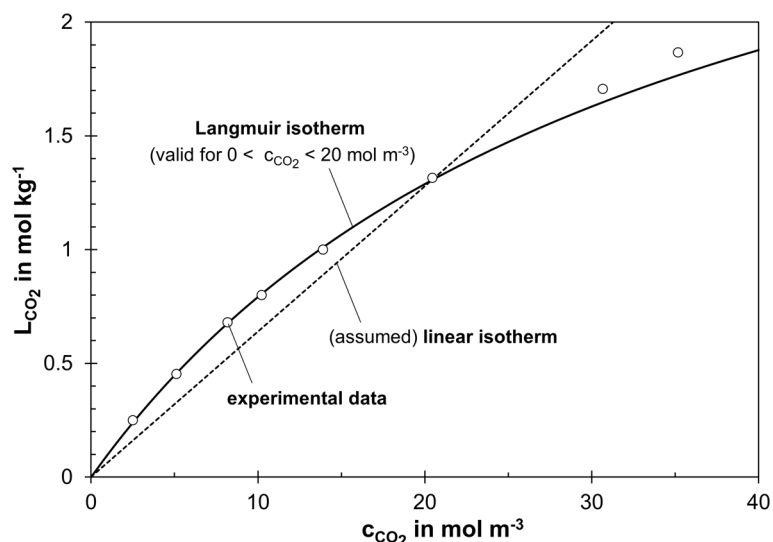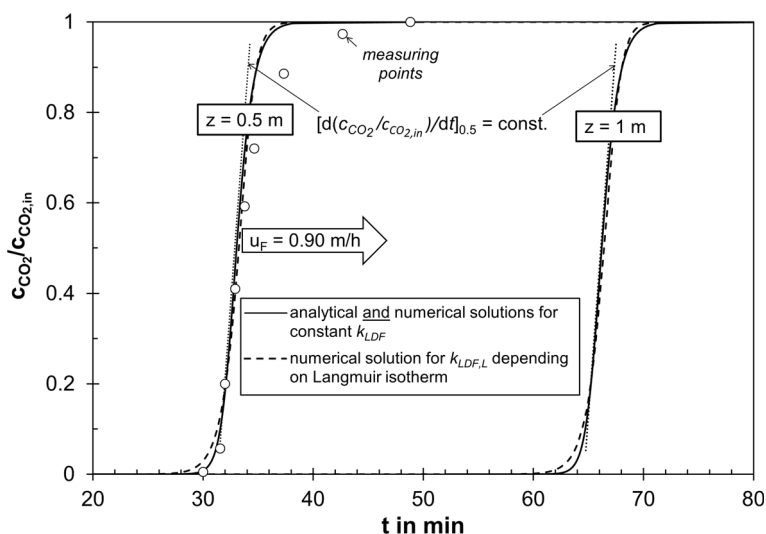
Figure 4. Langmuir adsorption isotherm for CO_2 on activated carbon (experimental data from [26]) and arbitrarily assumed linear adsorption isotherm used in Sect. 4 for the modeling of ad- and desorption in case of a linear adsorption isotherm.

Table 2. Data of isothermal ad- and desorption of CO_2 on activated carbon (Langmuir adsorption isotherm in Fig. 4; 10 bar, 25 °C; desorption with pure He; data from [26]).

Parameter	Value (10 bar total pressure, 20 °C)	Unit
A_{BET}	1.15×10^6	$m^2 kg^{-1}$
$c_{CO_2,0}$, $c_{CO_2,in}$	20.44 (adsorption for 5 vol % CO_2 in He and 10 bar total pressure)	$mol\,m^{-3}$
d_p	0.00125 (spherical particles)	m
d_{pore}	$= 4\,A_{BET}/(\varepsilon_p \rho_p) = 1.8 \times 10^{-9}$	m
D_{mol}	56×10^{-7}	$m^2 s^{-1}$
D_{Kn}	4.7×10^{-7}	$m^2 s^{-1}$
D_{pore}	4.4×10^{-7}	$m^2 s^{-1}$
$D_{eff,pore}$	0.6×10^{-7}, Eq. (26)	$m^2 s^{-1}$
$k_{ad,L}$	0.1027	$m^3 kg^{-1}$
$K_{ad,L}$	0.0297	$m^3 mol^{-1}$
$k_{LDF,L}$ [a]	$\approx 0.028 + 0.00135\,c_{CO_2}^{1.14}$ (based on Eq. (25); deviation < 1 %) [a]	s^{-1}
k_{LDF}	0.047 (const. mean value reached for $0.5\,c_{CO_2,in}$)	s^{-1}
L	0.5 (experimental value); 1 and 1.5 (values used for modeling)	m
u_s	0.00765	$m\,s^{-1}$
$L_{mol,m,max}$, $L_{mol,m,0}$	1.306 (max. loading for adsorption, initial loading for desorption)	$mol_{CO_2} kg^{-1}$
R	0.622, Eq. (16)	–
u_F	0.000251	$m\,s^{-1}$
ε_{bed}	0.41	–
ε_p	0.42	–
ρ_{bed}	470	$kg\,m^{-3}$
ρ_p	820	$kg\,m^{-3}$
τ_p	3	–

[a] Equation is valid for c_{CO_2} in $mol\,m^{-3}$ and only accurate for $c_{CO_2} < 20\,mol\,m^{-3}$.

Figure 5. Isothermal adsorption of CO_2 for a Langmuir adsorption isotherm. Eqs. (11)–(14) were solved numerically for a constant k_{LDF} and for $k_{LDF,L}$ according to Eq. (25). The numerical and analytical solution [22], Eqs. (15)–(17), and (19), perfectly fit for constant k_{LDF} and are indistinguishable (experimental data from [26]; parameters see Tab. 2).

different times are shown in Fig. S1 and profiles of c_{CO_2} and of $L_{mol,m}$ in Fig. S2 in Sect. 4 of the Supporting Information.

The deviation of the numerical solution, if the influence of the slope of the Langmuir adsorption isotherm on $k_{LDF,L}$ is

considered (Eq. (25)), from the solution with constant k_{LDF} is very small (Fig. 5). Here, $k_{LDF,L}$ increases from $0.028\,s^{-1}$ for $c_{CO_2} = 0$ to $0.07\,s^{-1}$ for $c_{CO_2} = 20.4\,mol\,m^{-3}$. Thus, the adsorption rate is lower/higher for low/high values of c_{CO_2} (Fig. 5), and the profiles of the CO_2 concentration with time (breakthrough curves) are due to this effect to a small extent different.

An explanation of the constant pattern behavior for a Langmuir adsorption is given in Fig. 6 by a simple schematic diagram, showing the dimensionless loading (L/L_{max}) and concentration of the adsorbed gas ($c_g/c_{g,in}$). Just for illustration, a simple "fictional" Langmuir adsorption isotherm, $L/L_{max} = 6c_g/c_{g,in}/(1 + 5c_g/c_{g,in})$, is assumed. Analogously to the heat regenerator, the adsorption process is regarded as a perpetually repeating two-step process: In a first step (1a), the c_g profile (initially a flat front) migrates into the bed by a small distance, leading to a shift from the profile of the loading of the solid adsorbent. This step accounts for the gas-solid mass transfer resistance. In the second step (1b), the adsorption equilibrium is established. With regard to a clear illustration, it is assumed that the (dimensionless) drop of c_g exactly equals the rise in loading, $\Delta(L/L_{max}) = \Delta(c_g/c_{g,in})$. Note that this just illustrating mass balance is not true for CO_2 adsorption at the given conditions and units for c and L (Tab. 2). For example,
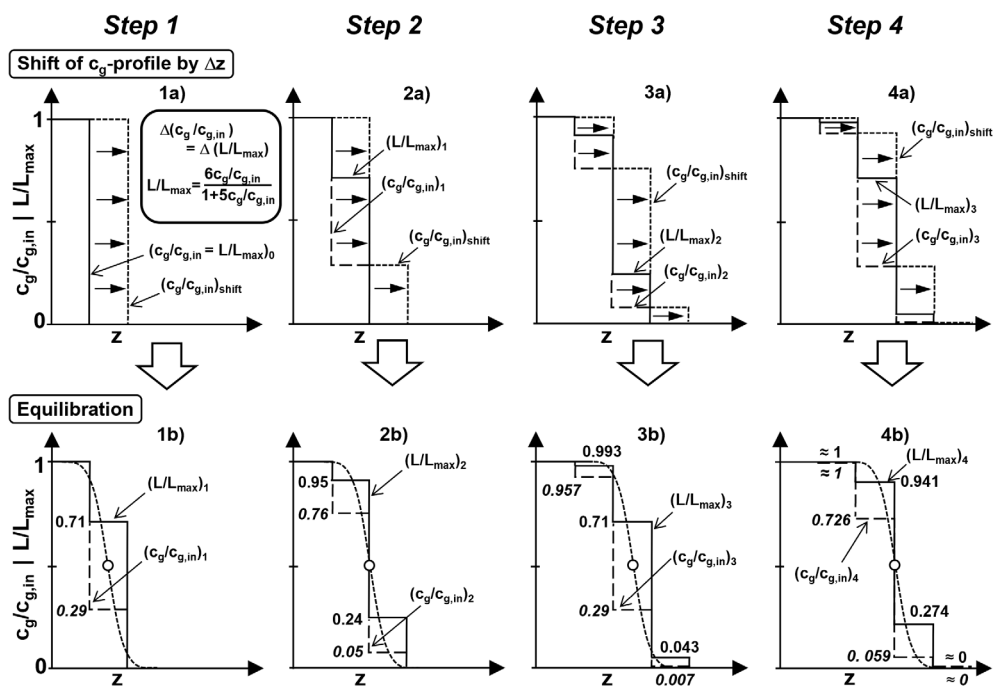
Figure 6. Explanation of constant pattern behavior for fixed-bed adsorption and Langmuir isotherm by a schematic diagram (c_g and L in dimensionless terms relative to inlet concentration of adsorbed gas $c_{g,in}$ and maximum loading L_{max}). A simple fictional Langmuir adsorption isotherm, $L/L_{max} = 6c_g/c_{g,in}/(1 + 5c_g/c_{g,in})$, is assumed. For a clear illustration, it is assumed that the (dimensionless) drop of c_g equals the rise in loading, $\Delta(L/L_{max}) = \Delta(c_g/c_{g,in})$. The adsorption is regarded as repeating two-step process (step 1a: shift between profiles of c_g and L (dashed and dotted-dashed lines); step 1b: adsorption equilibrium (solid lines). This two-step process is then repeated (2a/2b, 3a/3b, 4a/4b).

$\Delta(L_{\text{mol,m}}/L_{\text{mol,m,max}}) \approx 0.0014$ for $\Delta(c_{\text{CO}_2}/c_{\text{CO}_2,\text{in}}) = 0.1$. The two-step process is then repeated. Fig. 6 shows that a constant pattern is rapidly reached and is well explained by this simple schematic diagram.

As expected for desorption and a Langmuir isotherm, the breakthrough curve is spreading (Fig. 7). The numerical solution was conducted both for a constant k_{LDF} and $k_{\text{LDF,L}}$ according to Eq. (25). The analytical solution (constant k_{LDF}) is also shown. The corresponding profiles of $c_{\text{CO}_2}/c_{\text{CO}_2,0}$ versus z for different desorption times are depicted in Fig. S3. A graphical explanation of spreading during desorption for a linear adsorption isotherm is given in Fig. S4.

Fig. 7 illustrates that the analytic solution of Ruthven [17], Eq. (20), is a fairly good approximation; only for high and low concentrations ($c_{\text{CO}_2}/c_{\text{CO}_2,0} > 0.8$; $c_{\text{CO}_2}/c_{\text{CO}_2,0} < 0.2$), there are distinct deviations from the "correct" numerical solution. As for adsorption, the difference of the numerical solutions for a constant and a concentration-dependent value of k_{LDF} is small.
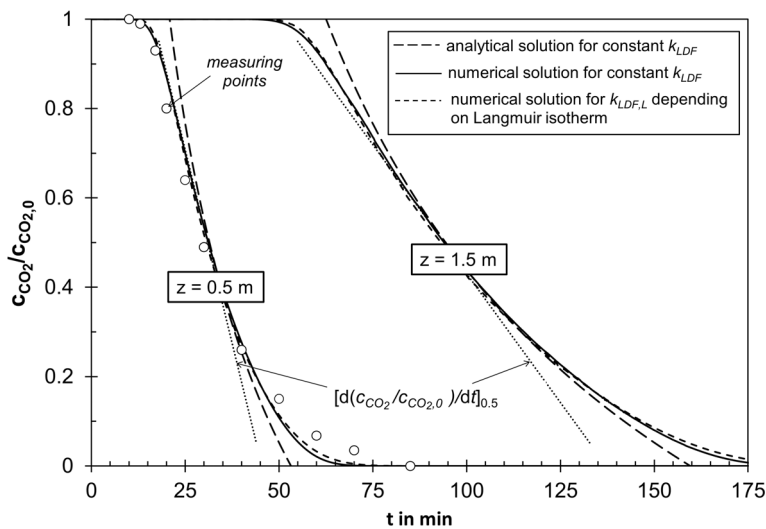
For a convex curved isotherm, as one may have for multi-layer adsorption, the adsorption front is spreading, but for desorption, there is a constant pattern [15, 20]. Hence, the behavior, not further discussed in this article, is the other way around as for the concave Langmuir isotherm.

4 Ad- and Desorption for a Linear Adsorption Isotherm

For a linear adsorption isotherm, the differential Eqs. (11) and (12) are still valid, but instead of the Eqs. (13) and (14) considering for Langmuir adsorption, one now has to use:

$$L^*_{\text{mol,m}} = K_{\text{ad,linear}}\, c_{\text{g}} \tag{27}$$

$$\bar{L}_{\text{mol,m}} = K_{\text{ad,linear}}\, \bar{c}_{\text{g,pore}} \tag{28}$$

Eqs. (11), (12), (27), and (28) lead to:

$$\frac{\partial \bar{L}_{\text{mol,m}}}{\partial t} = k_{\text{LDF}}\, K_{\text{ad}} \left(L^*_{\text{mol,m}} - \bar{L}_{\text{mol,m}} \right) =$$
$$\frac{\partial \bar{L}_{\text{mol,m}}}{\partial \bar{c}_{\text{g,pore}}} \frac{\partial \bar{c}_{\text{g,pore}}}{\partial t} = K_{\text{ad,linear}}\, \frac{\partial \bar{c}_{\text{g,pore}}}{\partial t} \tag{29}$$

$$\varepsilon_{\text{bed}} \frac{\partial c_{\text{g}}}{\partial t} + u_{\text{s}} \frac{\partial c_{\text{g}}}{\partial z} = -\rho_{\text{bed}}\, k_{\text{LDF}}\, K_{\text{ad,linear}} \left(c_{\text{g}} - \bar{c}_{\text{g,pore}} \right) \tag{30}$$

The approach for the heat regenerator, Eqs. (5)–(9), can be transferred to adsorption with a linear isotherm due to the similarity of the structure of the differential Eqs. (3) and (30). The standard deviation of the S-shaped adsorption front is:

$$\sigma_{\text{ad}} = t \sqrt{\frac{2\, u_{\text{s}}}{L} \frac{1}{\rho_{\text{bed}}\, k_{\text{LDF}}\, K_{\text{ad, linear}}}} =$$
$$\sqrt{\frac{2\, L\, u_{\text{s}}}{u_{\text{F}}^2} \frac{1}{\rho_{\text{bed}}\, k_{\text{LDF}}\, K_{\text{ad,linear}}}} \tag{31}$$

The velocity of the adsorption front and, thus, the position of the c-profile for $c_{\text{g}} = 0.5 c_{\text{g,in}}$ are:

$$u_{\text{F}} \approx \frac{u_{\text{s}}\, c_{\text{g,in}}}{\rho_{\text{bed}}\, L_{\text{mol,m,max}}} = \frac{u_{\text{s}}}{\rho_{\text{bed}}\, K_{\text{ad,linear}}} \tag{32}$$

By substitution of Eq. (32) in Eq. (31) it follows:

$$\sigma_{\text{ad}} = \sqrt{\frac{2\, L\, (u_{\text{F}}\, \rho_{\text{bed}}\, K_{\text{ad,linear}})}{u_{\text{F}}^2} \frac{1}{\rho_{\text{bed}}\, k_{\text{LDF}}\, K_{\text{ad,linear}}}}$$
$$= \sqrt{\frac{2\, L}{u_{\text{F}}} \frac{1}{k_{\text{LDF}}}} \sim \sqrt{\frac{L}{u_{\text{F}}}} \tag{33}$$

For $c_{\text{g}} = 0.5 c_{\text{g,in}}$, the slope of c_{g} with t at the axial reference position $z_{0.5}$ is:

$$\left(\frac{\partial \left(\frac{c_{\text{g}}}{c_{\text{g,in}}} \right)}{\partial t} \right)_{0.5} = \frac{1}{2.5\, \sigma_{\text{ad}}} = \frac{1}{2.5 \sqrt{2}} \sqrt{\frac{u_{\text{F}}\, k_{\text{LDF}}}{z_{0.5}}} \tag{34}$$

and for the slope with z (with reversed sign) for a given refernce time $t_{0.5}$ we have ($\mathrm{d}z = u_{\text{F}}\mathrm{d}t$):

$$\left(\frac{\partial \left(\frac{c_{\text{g}}}{c_{\text{g,in}}} \right)}{\partial z} \right)_{0.5} =$$
$$-\left(\frac{\partial \left(\frac{c_{\text{g}}}{c_{\text{g,in}}} \right)}{u_{\text{F}}\, \partial t} \right)_{0.5} = -\frac{1}{2.5 \sqrt{2}} \sqrt{\frac{k_{\text{LDF}}}{u_{\text{F}}\, z_{0.5}}} \tag{35}$$

Because of the lack of experimental data of a strictly linear isotherm, an arbitrary but reasonable value for $K_{\text{ad,linear}}$ of $0.064\ \text{m}^3\text{kg}^{-1}$ is chosen, as the

Figure 7. Desorption of CO_2 for Langmuir isotherm (parameters in Tab. 2). Eqs. (11)–(13) were solved numerically for constant k_{LDF} and $k_{\text{LDF,L}}$ according to Eq. (25). Analytical solution, Eq. (20) [17], is shown for constant k_{LDF}, experimental data from [24]. $\left| \mathrm{d}(c_{\text{CO}_2}/c_{\text{CO}_2,0})/\mathrm{d}t \right| = 0.035\ \text{min}^{-1}$ (0.5 m) and $0.012\ \text{min}^{-1}$ (1.5 m), as expected by Eq. (23) ($\sim 1/z_{0.5}$).

same loading is then reached as for Langmuir adsorption and a CO_2 concentration of 22.4 mol m^{-3}; see Fig. 4. All other parameters were kept constant as for the calculations for the case of Langmuir adsorption (Tab. 2).

The numerically and analytically derived breakthrough curves for three adsorber lengths coincide excellently (Fig. 8). As expected, the front is spreading with an increase of the *HTZ* proportional to $\sqrt{z_{0.5}}$. The *c*-profiles at different times are displayed in Fig. S5 and an explanation of spreading in Fig. S6 of Sect. S5. A method to calculate the *HTZ* is given in Sect. S6. The equations for ad- and desorption for a linear isotherm just yield mirror images; see also section S6. Desorption is therefore here not further discussed.
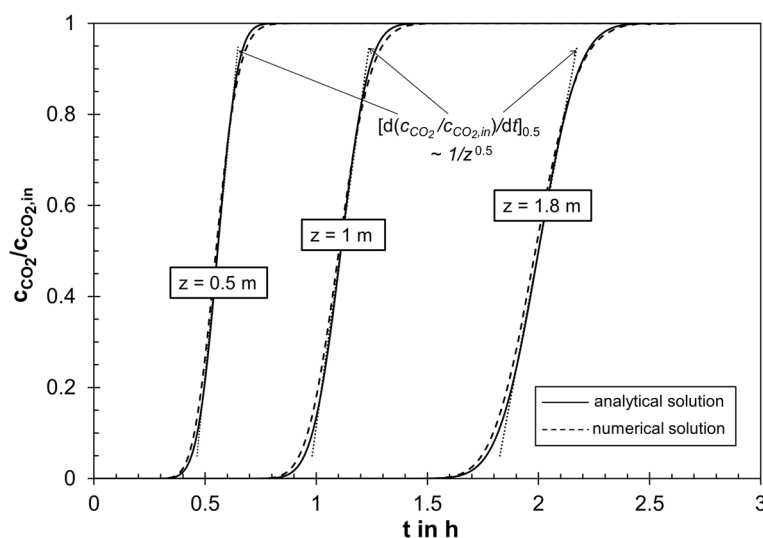
5 Regeneration of a Coked Catalytic Fixed Bed

5.1 Isothermal Decoking of a Fixed-Bed Catalyst

The differential equation for the mass balance of coke burn-off of an initially uniformly coked catalyst in a fixed-bed reactor is as follows:

$$\varepsilon_{\text{bed}} \frac{\partial c_{O_2}}{\partial t} + u_s \frac{\partial c_{O_2}}{\partial z} = -k_m \, \rho_{\text{bed}} \, c_{O_2} \, \bar{L}_C \tag{36}$$

Eq. (36) presumes that the rate of coke burn-off is first order with regard to the concentration of O_2 in the bulk phase and to the mean carbon load. For isothermal decoking, the rate constant k_m is here considered as constant, $k_m \neq f(\bar{L}_C)$. This implies that local gradients of the carbon load and the concentration of O_2 in the particles are negligible. If pore diffusion distinctly affects the rate, as one may have for $T > 450\,°C$ and $d_p > 2$ mm [12, 28, 29], an effective value $k_{m,\text{eff}}$ depending on

the mean values of $\bar{L}_C$ and $\bar{c}_{O_2}$ is needed. The solution of Eq. (36) is then much more complicate, but this aspect is beyond the scope of this article.

In addition, the temperature and thus k_m usually rise during coke burn-off in a fixed bed. Then, a heat balance and the influence of temperature on k_m have to be considered (see Sect. 5.2). However, at first the isothermal case with constant value of k_m is inspected, particularly because the derived equations are useful for other fluid-solid systems with a negligible *T*-change. In the isothermal case, only a reaction and not a heat front moves through the bed. The starting point for an analytical solution of the coke burn-off process is the assumption that the S-shaped profiles of *C* load and O_2 concentration are almost, but never exactly mirror images:

$$\bar{L}_{C,m} = \left(1 - k_{\text{offset}} \frac{c_{O_2}}{c_{O_2,\text{in}}}\right) L_{c,0} \tag{37}$$

The parameter k_{offset} considers the shift of both profiles in axial direction, e.g., the position $z_{0.5}$, where $0.5L_{C,0}$ and $0.5c_{O_2,0}$ are reached. Here, a starting value of 0.99 for k_{offset} is used to account for a slightly lower C load compared to a "perfect" mirror image; for example, $L_C/L_{C,0} = 0.505$ for $c_{O_2}/c_{O_2,0} = 0.5$. Eqs. (36) and (37) yield:

$$\varepsilon_{\text{bed}} \frac{\partial c_{O_2}}{\partial t} + u_s \frac{\partial c_{O_2}}{\partial z} =$$
$$- k_m \, \rho_{\text{bed}} \, c_{O_2} \left(1 - k_{\text{offset}} \frac{c_{O_2}}{c_{O_2,\text{in}}}\right) L_{c,0} \tag{38}$$

$$-u_s \frac{\partial c_{O_2}}{\partial z} = k_m \, \rho_{\text{bed}} \, L_{c,0} \left(c_{O_2} - k_{\text{offset}} \frac{c_{O_2}^2}{c_{O_2,\text{in}}}\right) \text{ for quasi-steady-state} \tag{39}$$

Integration of Eq. (39), representing quasi-steady-state, and rearrangement leads to:

$$\frac{c_{O_2}}{c_{O_2,\text{in}}} = \left\{ k_{\text{offset}} + [1 - k_{\text{offset}}] \exp\left(\frac{k_m \, \rho_{\text{bed}} \, L_{c,0}}{u_s} z\right) \right\}^{-1} \tag{40}$$

For $k_{\text{offset}} = 0.99$, Eq. (40) yields:

$$\frac{c_{O_2}}{c_{O_2,\text{in}}} = \left\{ 0.99 + 0.01 \exp\left(\frac{k_m \, \rho_{\text{bed}} \, L_{c,0}}{u_s} z\right) \right\}^{-1} \tag{41}$$

Fig. 9 shows the c_{O2} and L_C profiles obtained by Eqs. (37) and (41). The dashed-dotted line (lower part) also displays the "perfect", but never reached mirror image, i.e., $L_C/L_{C,0} = 1 - c_{O_2}/c_{O_2,0}$. The slope derived by derivation of Eq. (41) for $z_{0.5} = 0.46$ m, corresponding to $c_{O_2} = 0.5c_{O_2,0}$, is:

Figure 8. Isothermal adsorption of CO_2 for a linear adsorption isotherm (Fig. 4). Eqs. (11), (12), (27), and (28) were solved numerically. The analytical solution is also shown: The gradient $(d[c_{CO_2}/c_{CO_2,\text{in}}]/dt)_{0.5}$ is calculated by Eq. (34), the time to reach $z_{0.5}$ by Eq. (32), and the CDF by Eqs. (S16) and (S18) based on σ_{ad}, Eq. (33) (parameters in Tab. 2).

$$\left(\frac{\partial \left(\frac{c_{O_2}}{c_{O_2,in}} \right)}{\partial z} \right)_{0.5} = -\frac{0.01\, C\, \exp(C\, z_{0.5})}{\{0.99 + 0.01\, \exp(C\, z_{0.5})\}^2} \qquad (42)$$

with $C = \dfrac{k_m\, \rho_{bed}\, L_{c,0}}{u_s}$

Based on the parameters listed in Tab. 3, $C = 10\,\mathrm{m}^{-1}$ and the slope (Eq. (42)) is $-2.5\,\mathrm{m}^{-1}$.
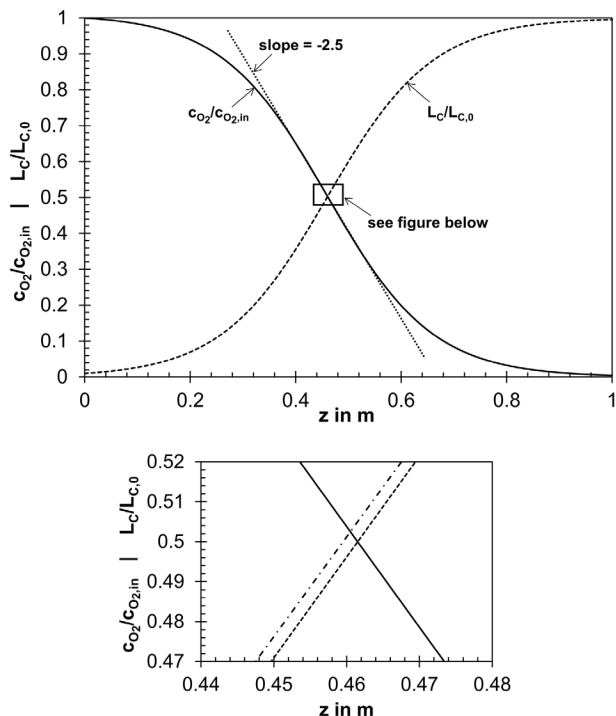
Figure 9. Profiles of c_{O_2} for isothermal coke burn-off (Eq. (41); quasi-steady-state; $k_{offset} = 0.99$; $C = 10\,\mathrm{m}^{-1}$, parameters in Tab. 3). The dashed-dotted line in the lower part shows a perfect mirror image for comparison, i.e., $L_C/L_{C,0} = 1 - c_{O_2}/c_{O_2,in}$.

Eq. (40) leads to the position of $z_{0.5}$, which depends on the offset factor and the parameter C:

$$z_{0.5} = \frac{1}{C}\, \ln\left(\frac{2 - k_{offset}}{1 - k_{offset}} \right) \qquad (43)$$

$z_{0.5}$ is 0.24 m for $k_{offset} = 0.9$, 0.46 m for $k_{offset} = 0.99$ (used here as example, Fig. 9), 0.92 m for $k_{offset} = 0.9999$, and 3.67 m for $k_{offset} = 1-1/10^{16}$ (limit for use of Eq. (43), as discussed below).

The velocity of the reaction front, deduced by a mass balance (O_2) for a volume element of the fixed bed [12, 28, 29], is:

$$u_F = \frac{u_s\, c_{O_2,in}}{\rho_{bed}\frac{L_{c,0}}{M_C} + \varepsilon_{bed}\, c_{O_2,in}} \approx \frac{u_s\, c_{O_2,in}\, M_C}{\rho_{bed}\, L_{c,0}} \qquad (44)$$

The position $z_{0.5}$ for a given time of regeneration and velocity of the reaction front is:

Table 3. Values used in this work to model the regeneration of a coked fixed-bed catalyst.

Parameter	Value	Unit
$c_{O_2,in}$ (1 % in N_2; 450 °C, 1 bar)	0.17	$\mathrm{mol\,m^{-3}}$
$c_{p,g,mol}$	30	$\mathrm{J\,mol^{-1}K^{-1}}$
$c_{s,m}$	1000	$\mathrm{J\,kg^{-1}K^{-1}}$
E_A (needed to calculate adiabatic coke burn-off)	100	$\mathrm{kJ\,mol}$
k_m (450 °C, used for isothermal burn-off)	0.1	$\mathrm{m^3kg^{-1}s^{-1}}$
$k_{m,0}$ (needed to calculate adiabatic burn-off)	1.68×10^6	$\mathrm{m^3kg^{-1}s^{-1}}$
$L_{C,0}$	0.1	$\mathrm{kg_C kg_{cat}^{-1}}$
P	1	bar
$T_g = T_s$ (isothermal burn-off)	450	°C
$T_{g,in} = T_{s,0}$ (adiabatic burn-off)	382	°C
u_F	0.073	$\mathrm{m\,h^{-1}}$
u_s (450 °C, 1 bar)	0.5	$\mathrm{m\,s^{-1}}$
$\Delta_R H$ (oxidation of coke/carbon to CO_2)	$-393\,000$	$\mathrm{J\,mol^{-1}}$
ε_{bed}	0.41	–
ρ_{bed}	500	$\mathrm{kg\,m^{-3}}$
$\rho_{g,mol}$ (1 bar, 450 °C)	17	$\mathrm{mol\,m^{-3}}$

$$z_{0.5} = u_F\, t_{reg} \qquad (45)$$

For the given conditions (Tab. 3), u_F is 0.073 m h^{-1}. Hence, the position depicted in Fig. 9 ($z_{0.5} = 0.46$ m) is reached after about 6 h.

According to Eq. (44), u_F increases proportionally to the gas velocity (u_s). Thus, the time needed for regeneration decreases proportionally with u_s, if the effect that the reaction front broadens is negligible ($L \gg HTZ$). Combining Eqs. (43)–(45) yields:

$$k_{offset} = \frac{\{2 - \exp\left(k_m c_{O_2,in} M_C t_{reg}\right)\}}{\{1 - \exp\left(k_m c_{O_2,in} M_C t_{reg}\right)\}};$$
valid for
$$k_m c_{O_2,in} M_C t_{reg} > \ln2, \text{ i.e., } k_{offset} > 0 \qquad (46)$$

For the given example and values listed in Tab. 3 one has:

$$k_{offset} = \frac{\{2 - \exp\left(0.73\, h^{-1}\, t_{reg}\right)\}}{\{1 - \exp\left(0.73\, h^{-1}\, t_{reg}\right)\}} \quad \text{for} \quad t_{reg} > 0.95\, h, \text{ i.e., } k_{offset} > 0 \qquad (47)$$

For $t_{reg} = 0.95$ h, k_{offset} is 0, for 2 h $k_{offset} = 0.7$, and for $t_{reg} > 8$ h, $k_{offset} = 1$, and $L_C/L_{C,0} \approx c_{O_2}/c_{O_2,0}$ (Fig. S7, Sect. S7). Combining Eqs. (40) and (46) yields the concentration front equation:

$$\frac{c_{O_2}}{c_{O_2,0}} = \left\{ \frac{\{2-\exp(k_m c_{O_2,in} M_C t_{reg})\}}{\{1-\exp(k_m c_{O_2,in} M_C t_{reg})\}} + \left[1 - \frac{\{2-\exp(k_m c_{O_2,in} M_C t_{reg})\}}{\{1-\exp(k_m c_{O_2,in} M_C t_{reg})\}} \right] \exp\left(\frac{k_m \rho_{bed} L_{c,0}}{u_s} z \right) \right\}^{-1} \quad (48)$$

Thus, instead of solving Eq. (36) numerically, Eq. (48) (combined with Eq. (37) to determine also the profile of $L_{C,m}$) can be used as approximate solution. For the given example it follows:
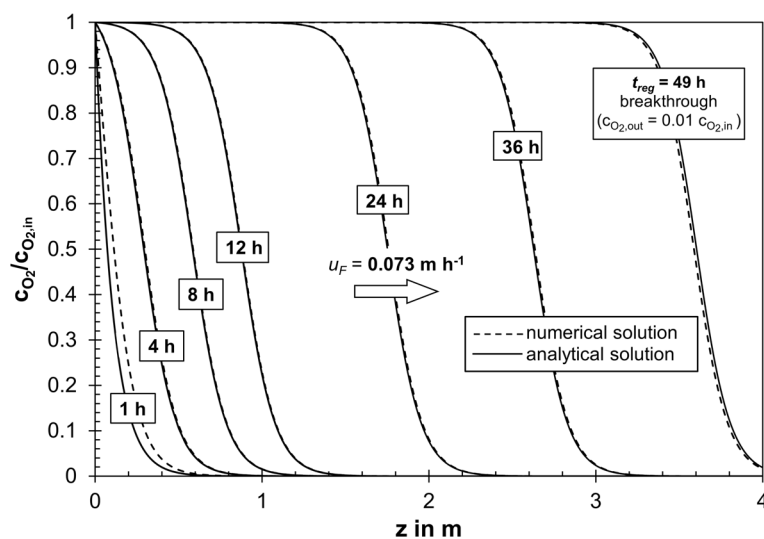
$$\frac{c_{O_2}}{c_{O_2,0}} = \left\{ \frac{\{2-\exp(0.73\ h^{-1}\ t_{reg})\}}{\{1-\exp(0.73\ h^{-1}\ t_{reg})\}} + \left[1 - \frac{\{2-\exp(0.73\ h^{-1}\ t_{reg})\}}{\{1-\exp(0.73\ h^{-1}\ t_{reg})\}} \right] \exp\left(\frac{10}{m} z \right) \right\}^{-1} \quad (49)$$

Eqs. (46) and (48) are not applicable for $k_m\ c_{O_2,in}\ M_C\ t_{reg} > 38$. Eq. (46) then leads to $k_{offset} = 1$, if a speadsheet (Excel) is used, and Eq. (48) fails. This limit is reached here for $t_{reg} \approx 51$ h. Fortunately, this is not relevant, as a constant pattern is already reached after 8 h (Figs. 10–13).
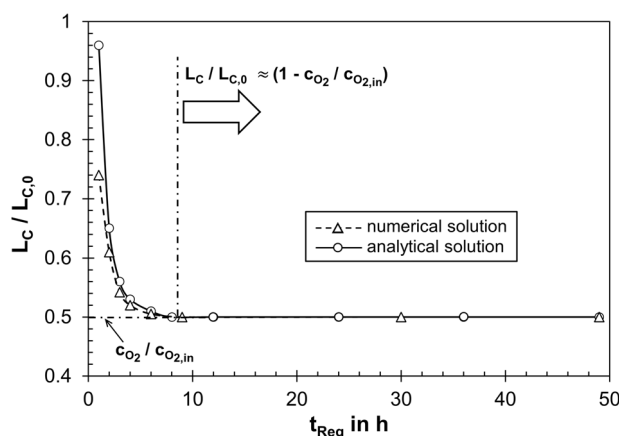
Eq. (48) can also be used to determine the constant HTZ; see Sect. S8.

A symmetrical S-shaped reaction front and constant pattern is reached after 4 h (Fig. 10). From then on, the analytical solution, Eq. (49), is an excellent approximation; only for $t_{reg} < 4$ h, we get deviations from the numerical "correct" solution. In this initial phase, a symmetrical S-shaped profile is not fully developed and not detached from the entrance of the bed.

A similar trend is depicted in Fig. 11 for the C load: Initially ($t_{reg} < 8$ h), the normalized load is appreciably higher than the respective value of the normalized O_2 concentration. The x-axis in Fig. 11 shows the time, when $c_{O_2} = 0.5 c_{O_2,0}$ is exactly reached. For $t_{reg} > 8$ h, the difference between $c_{O_2}/c_{O_2,in}$ and

Figure 11. Normalized C-load during isothermal coke burn-off for the regeneration time, when $c_{O_2} = 0.5 c_{O_2,0}$ is exactly reached (numerical solution of Eq. (36) and analytical solution by Eqs. (37), (47), and (49)). Triangles and circles are only guide for the eye. For $t_{reg} < 0.95$ h (Fig. S7), $k_{offset} < 0$ and $L_C/L_{C,0} > 1$, which is physically nonsensical.

$L_C/L_{C,0}$ almost vanishes, both for the numerical and analytical solution.

After about 8 h coke burn-off, a constant value of the HTZ is achieved (Figs. 12 and 13). Complementary to Fig. 10, the profiles of C load, almost mirror images of the c_{O_2} profiles, are displayed in Fig. S8. The constant pattern behavior is explained in Fig. S9 by a schematic diagram.

5.2 Adiabatic Decoking of a Fixed–Bed Catalyst

Usually, catalyst regeneration by coke burn-off in a fixed bed is conducted adiabatically, and in addition to the mass balance (Eq. (36)) the following heat balance is then also needed:
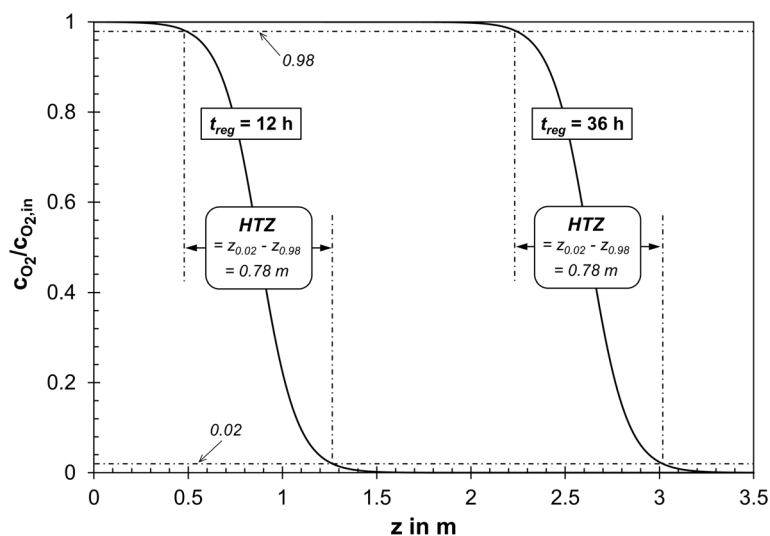
$$\left(\rho_{bed}\ c_{s,m} + \varepsilon_{bed}\ \rho_{g,mol}\ c_{P,g,mol} \right) \frac{\partial T}{\partial t} = -u_s \rho_{g,mol}\ c_{P,g,mol} \frac{\partial T}{\partial z} - k_m\ \rho_{bed}\ c_{O_2}\ \bar{L}_C\ \Delta_R H \quad (50)$$

The influence of temperature on k_m is given by the well-known Arrhenius equation:

$$k_m = k_{m,0}\ \exp\left(\frac{-E_A}{R\ T} \right) \quad (51)$$

The kinetic parameters E_A and $k_{m,0}$ (Tab. 3) are rounded values based on own measurements [12, 28, 29]. Again note that the influence of pore diffusion on the effective rate constant is here not considered. The gas-solid temperature difference is also neglected, as this ΔT is here less than 10 K. The same holds true for the negligible impact of axial heat dispersion [12, 28, 29].

The adiabatic temperature increase (for a steady-state process) is:

Figure 10. Normalized O_2 profiles for isothermal coke burn-off calculated by Eq. (49) and numerically by solution of Eq. (36) for different regeneration times (parameters in Tab. 3).

Figure 12. Profiles of normalized c_{O2} during isothermal coke burn-off, calculated by Eq. (49) at t_{reg} of 12 h and 36 h underlining the constant pattern of the burn-off process (parameters in Tab. 3; HTZ defined as distance of positions, where 0.02 and 0.98 $c_{O_2,0}$ are reached).
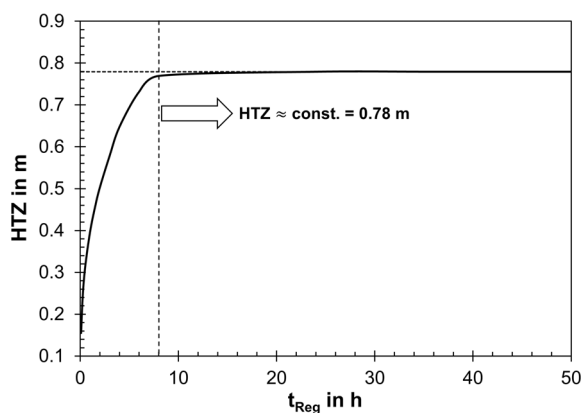
Figure 13. Influence of regeneration time (isothermal burn-off) on the HTZ, defined as distance of positions, where $0.02c_{O2,in}$ and $0.98c_{O2,in}$, respectively, are reached (see Fig. 12).

$$\Delta T_{ad} = \frac{c_{O_2,in} \, |\Delta_R H|}{\rho_{g,mol} \, c_{p,g,mol}} \tag{52}$$

ΔT_{ad} for coke burn-off is large, about 130 K even for only 1 % O_2 (rest N_2) in the feed gas.

During transient coke burn-off, an overheating above the adiabatic steady-state temperature rise ΔT_{ad}, Eq. (52) arises. To quantify this effect, the heat balance for the reaction zone is instructive, whereby the originator of the balance "moves" forward with the velocity of the front u_F:

$$Q_r = Q_g - Q_s \tag{53}$$

The heat flux produced by the coke burn-off is:

$$Q_r = (u_g - u_F) \, A_R \, \varepsilon_{bed} \, c_{O_2,in} \, |\Delta_R H| = (u_g - u_F) \, A_R \, \varepsilon_{bed} \, \Delta T_{ad} \, \rho_{g,mol} \, c_{p,g,mol} \tag{54}$$

The heat flux needed to heat up the gas from $T_{g,in}$ up to the maximum temperature reached at the end of the reaction front $T_{F,max}$ is:

$$Q_g = (u_g - u_F) \, A_R \, \varepsilon_{bed} \, \rho_{g,mol} \, c_{p,g,mol} (T_{F,max} - T_{g,in}) \tag{55}$$

The heat flux conceptually entering the zone by the hot particles from the viewpoint of a moving observer is:

$$Q_s = u_F \, A_R \, \varepsilon_{bed} \, \rho_{bed} \, c_{s,m} (T_{F,max} - T_{g,in}) \tag{56}$$

Eqs. (53)–(56) and the correlation $u_s = \varepsilon_{bed} u_g$ yield the temperature increase reached during the unsteady-state coke burn-off process:

$$\Delta T_F = T_{F,max} - T_{g,in} =$$
$$\Delta T_{ad} \left(1 - \frac{u_F}{(u_s - \varepsilon_{bed} \, u_F)} \frac{\rho_{bed} \, c_{s,m}}{\rho_{g,mol} \, c_{p,g,mol}} \right)^{-1} \tag{57}$$

The lower L_C, the higher u_F (Eq. (44)) and the higher the overheating above the stationary ΔT_{ad}. For the given conditions (Tab. 3), this effect is small: $\Delta T_F = T_{ad}$, i.e., $\Delta T_F - \Delta T_{ad} = 5$ °C.

The profiles of oxygen concentration and temperature during adiabatic and isothermal coke burn-off are compared in Fig. 14. The chosen temperature for isothermal burn-off (450 °C) is exactly the mean value of the adiabatic case (382 °C < T < 518 °C), and the reaction rate is therefore lower for adiabatic operation compared to isothermal until 450 °C are reached, and then higher. In both cases, we have a constant pattern, but in the front section of the reaction zone, the drop of c_{O_2} is more pronounced for isothermal operation ($T > T_{adiabatic}$); in the rear section, this is reverse. This leads to an asymmetrical c_{O_2} profile for adiabatic operation.

The velocity of the front u_F is the same in both cases (Fig. 14). Only the position $z_{0.5}$ for $c_{O_2} = 0.5c_{O_2,in}$ reached after a certain time is slightly displaced by an offset of 0.1 m for isothermal and adiabatic operation. The reason is the asymmetrical adiabatic front compared to the ideally S-shaped isothermal profile. Nevertheless, Fig. 14 shows that the adiabatic process can be at least approximated by the isothermal operation equation (Eq. (48)), if the adiabatic mean temperature (= $T_{g,in} + 0.5\Delta T_{ad}$), calculated by Eq. (52), is used. This procedure is at least suitable for a baseline estimate of the regeneration process.

It should be finally mentioned that reliable experimental data of both isothermal and adiabatic catalyst regeneration in a fixed bed have unfortunately, to our best knowledge, until now almost not been published and could here not be compared with the numerical and analytical solutions. Isothermal coke burn-off in a fixed bed with a certain length of, e.g., 1 m by external cooling is practically impossible, even for a lab-scale reactor with a small diameter. The same holds true for an adiabatic lab-scale reactor operation, as the ratio of the external surface to the reactor volume is high, and an efficient insulation to avoid heat losses is not visible.
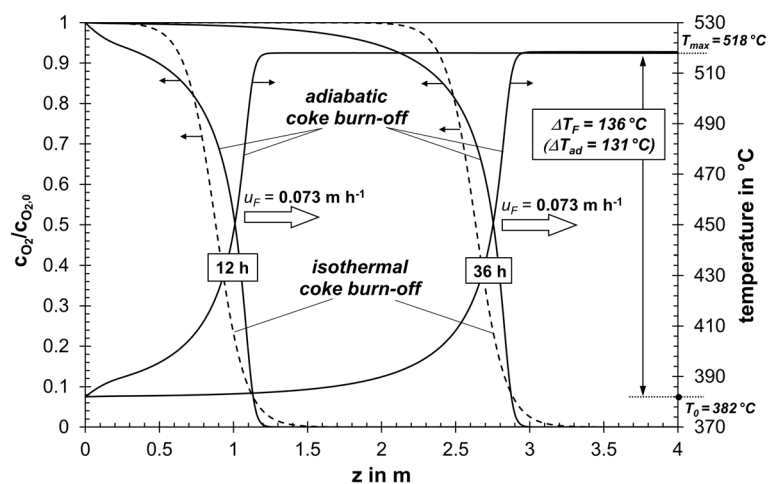
Figure 14. Adiabatic and isothermal catalyst regeneration by coke burn-off calculated by the numerical solution of the Eqs. (36) and (50) (parameters in Tab. 3). Reliable experimental data are almost not available (see text) and therefore not shown for comparison.

Published data of industrial reactors with an always almost adiabatically conducted regeneration are also rare. We here just refer to own previous publications [12, 28, 29], where the com-parison of modeling with data of an industrial reactor for reforming of low-octane gasoline shows that the adiabatic modeling of the catalyst regeneration by coke burn-off is reliable.

The equations given here for the coke burn-off process are also valid for other unsteady-state gas-solid fixed-bed systems, such as oxidation/reduction of metals/metal oxides or of catalysts with a metal as active component, at least for a first-order reaction both with regard to the concentration of the gaseous and solid reactant. We have planned to conduct respective measurements of such reaction systems to (im)prove the analysis derived here further.

6 Conclusion

The analysis and design of unsteady-state fixed-bed processes such as heat regeneration, adsorption and desorption, and gas-solid reactions is very complex, above all the determination of the type and height of the mass and/or heat transfer zone. In this review, the current status of numerical as well as suitable analytical solutions is presented. The main characteristics of these unsteady-state fixed-bed processes are summarized in Tab. 4.

Table 4. Main characteristics of unsteady-state fixed-bed processes.

Unsteady-state fixed-bed process		Parameter (P) $P = f(z)$	Height of transfer zone	(Approximate) analytical solution [source]
Heat regenerator		T_{fl} (+/−)	Dispersive $HTZ \sim \sqrt{z}$	Eqs. (5), (8), (9), (S1)–(S3) [4, 5]
		T_s (+/−)		
Adsorption[a]	Langmuir isotherm	c_g (−)	Const. pattern	Eq. (15) [22]
		$L_{mol,m}$ (−)	HTZ = const.	
	Linear isotherm		Dispersive $HTZ \sim \sqrt{z}$	Eqs. (31), (35), (S16), (S18), and (S20) [this work]
Desorption[a]	Langmuir	c_g (+)	Dispersive $HTZ \sim z$	Eq. (20) [17]
		$L_{mol,m}$ (+)		
	Linear isotherm		Dispersive $HTZ \sim \sqrt{z}$	Eqs. (31), (35), (S17), (S19), and (S21) [this work]
Fluid-solid reaction (example of coke burn-off)	Isothermal	c_{O_2} (−)	Const. pattern	Eq. (48) [this work]
		L_C (+)	HTZ = const.	
	Adiabatic	c_{O_2} (−)	Const. pattern	None (numerical solution needed); only baseline estimate by Eq. (48) and $T_{mean,ad}$ (Eq. (52))
		L_C (+)	HTZ = const.	
		T_g (+)		
		T_s (+)		

[a] Isothermal ad/desorption of a single gaseous component with concentration c_g.
(+) indicates a parameter increasing in the (heat/mass) transfer zone in the direction of fluid flow, (−) the reverse, and (+/−) indicates that the temperatures of both fluid and solid in a packed-bed heat regenerator increase/decline for an initially hot/cold fixed bed and a cold/hot gas.

Only two cases of those considered here lead to a constant pattern behavior (constant *HTZ*), namely, adsorption for a Langmuir adsorption isotherm and isothermal as well as adiabatic coke burn-off during catalyst regeneration, here used as an instructive example of a gas-solid reaction. In the first case, the constant pattern is the result of the convex curvature of the Langmuir adsorption isotherm, whereas for coke burn-off, this is the result of the mirror image of the S-shaped profiles of carbon loading and O_2 concentration, respectively, in the reaction zone. In all other cases (heat regenerator, adsorption for linear isotherm, desorption for Langmuir and linear isotherm) the transfer zone is dispersive, and the height of the zone increases with greater length of the fixed bed.

The equations recommended in this work as suitable, partly approximate solutions for the axial profiles of temperature (heat regenerator) or of gas concentration (sorption, coke burn-off), three selected from literature and three developed in this work, are listed in Tab. 4.

Supporting Information

Acknowledgment

Symbols used

a_V	[m²m⁻³]	external surface of particles per volume of heat regenerator
A_{BET}	[m²kg⁻¹]	BET surface area
A_R	[m²m⁻³]	cross-sectional area of fixed bed
c_{CO_2}	[mol m⁻³]	concentration of CO_2
$c_{CO_2,in}$	[mol m⁻³]	initial concentration of CO_2 at entrance of fixed bed during adsorption
$c_{CO_2,0}$	[mol m⁻³]	concentration of CO_2 in a uniformly saturated fixed bed
c_g	[mol m⁻³]	concentration of adsorbed gas
$c_{g,0}$	[mol m⁻³]	concentration of gas in uniformly saturated bed
$\bar{c}_{g,pore}$	[mol m⁻³]	mean concentration of gas in the pores
c_{O_2}	[mol m⁻³]	concentration of oxygen
$c_{O_2,in}$	[mol m⁻³]	inlet concentration of oxygen at entrance of fixed–bed
$c_{p,g,mol}$	[J mol⁻¹K⁻¹]	heat capacity of gas
$c_{s,m}$	[J kg⁻¹K⁻¹]	heat capacity of solid
d_p	[m]	particle diameter
d_{pore}	[m]	(mean) pore diameter; $d_{pore} = 4 A_{BET} \left(\varepsilon_p \rho_p \right)^{-1}$

$D_{eff,ad}$	[m²s⁻¹]	effective diffusion coefficient (CO_2/He) for Langmuir adsorption (Eq. (25))
D_{mol}	[m²s⁻¹]	molecular diffusion coefficient (CO_2/He)
D_{Kn}	[m²s⁻¹]	Knudsen diffusion coefficient (CO_2/He); $\approx 0.7 \{8RT/(\pi M)\}^{0.5} d_{pore}$
$D_{eff,pore}$	[m²s⁻¹]	effective pore diffusion coefficient (CO_2/He), Eq. (26)
E_A	[J mol⁻¹]	activation energy of reaction of coke burn-off
$\Delta_R H$	[J mol⁻¹]	enthalpy of coke/carbon oxidation (to CO_2)
HTZ	[m]	height of transfer zone
$k_{ad,L}$	[m³kg⁻¹]	parameter of Langmuir isotherm, Eq. (13)
k_{LDF}	[s⁻¹]	(constant) mass transfer coefficient (linear driving force model, Eq. (12))
$k_{LDF,L}$	[s⁻¹]	mass transfer coefficient (Langmuir adsorption, Eq. (25))
k_m	[m³kg⁻¹s⁻¹]	(effective) rate constant of coke burn-off (assumed as independent of L_C)
$k_{m,0}$	[m³kg⁻¹s⁻¹]	pre-exponential factor of k_m
k_{offset}	[–]	factor in Eq. (37)
$K_{ad,linear}$	[m³kg⁻¹]	adsorption constant of linear isotherm, Eq. (27)
$K_{ad,L}$	[m³mol⁻¹]	adsorption constant of Langmuir adsorption isotherm (see Eq. (13))
L	[m]	length of fixed bed
$\bar{L}_C$	[kg kg⁻¹]	mean carbon load (kg carbon per kg catalyst)
$L_{C,0}$	[kg kg⁻¹]	initial carbon load (kg carbon per kg catalyst)
$L^{\star}_{mol,m}$	[mol kg⁻¹]	loading of solid with adsorbed gas
$\bar{L}_{mol,m}$	[mol kg⁻¹]	loading of solid with adsorbed gas for $c_g = \bar{c}_{g,pore}$
$L_{mol,m,max}$	[mol kg⁻¹]	maximum loading of solid with adsorbed gas for $c_g = c_{g,in}$
M_C	[kg mol⁻¹]	molar mass of coke (carbon)
Q_g	[J s⁻¹]	heat flux to heat up the gas phase (coke burn-off)
Q_r	[J s⁻¹]	heat flux produced by coke burn-off
Q_s	[J s⁻¹]	heat flux entering reaction zone by heated solid
R	[–]	parameter of Langmuir adsorption isotherm, Eq. (16)
R_i	[m³K W⁻¹]	heat transfer resistance (see Sect. S.2)
$t_{0.5}$	[s]	time needed for center of transfer zone to reach reference position $z_{0.5}$
t_{reg}	[s]	regeneration time
ΔT_{ad}	[°C, K]	(stationary) adiabatic temperature rise (coke burn-off)
ΔT_F	[°C, K]	unsteady-state temperature rise within reaction front (coke burn-off)
T_{fl}	[°C, K]	temperature of fluid
$T_{F,max}$	[°C, K]	maximum temperature of reaction front (coke burn-off)
T_g	[°C, K]	temperature of gas

$T_{g,0}$	[°C, K]	initial (inlet) temperature of gas
$T_{mean,ad}$	[°C, K]	mean temperature of adiabatic coke burn-off
T_s	[°C, K]	temperature of solid
u_F	[m s^{-1}]	velocity of (heat, adsorption, reaction) front
u_g	[m s^{-1}]	interstitial gas velocity
u_s	[m s^{-1}]	superficial gas velocity
z	[m]	axial coordinate in fixed bed (in direction of fluid flow)
$z_{0.5}$	[m]	(reference) position in fixed bed, where the center of the transfer zone is located

Greek letters

α_{ex}	[W m^{-2}s^{-1}]	heat transfer coefficient (external gas-solid heat transfer)
ε_{bed}	[–]	porosity of fixed bed
ε_P	[–]	porosity of particle
Θ_g, Θ_s	[–]	dimensionless temperature (difference) of gas and solid, see Fig. 3
$\lambda_{eff,ax}$	[W m^{-1}K^{-1}]	effective axial thermal conductivity in fixed bed (Sect. S2)
λ_g	[W m^{-1}K^{-1}]	thermal conductivity of gas (Sect. S2)
λ_s	[W m^{-1}K^{-1}]	thermal conductivity of particle (Sect. S2)
ρ_{bed}	[kg m^{-3}]	bulk density of fixed bed
$\rho_{g,mol}$	[mol m^{-3}]	density of gas
ρ_P	[kg m^{-3}	density of particle
σ_{ad}	[s]	standard deviation of sorption front for linear isotherm, Eq. (33)
σ_T	[s]	standard deviation of temperature front, Eq. (5)
σ_i^2	[s^2]	variance (of temperature or adsorption profile)
τ_g	[m s^{-1}]	(interstitial) residence time of gas in the fixed bed
τ_P	[–]	tortuosity of particle

Abbreviations

CDF	(Gaussian) cumulative distribution function
DE	differential equation

References

[1]   A. Anzelius, *Z. Angew. Math. Mech.* **1926**, *6*, 291–294. DOI: https://doi.org/10.1002/zamm.19260060404

[2]   W. Nusselt, *Z. Ver. Dtsch. Ing.* **1927**, *71*, 85–91.

[3]   M. Jakob, *Heat Transfer*, Wiley, New York **1957**, Vol. 3, Chap. 34.

[4]   O. Levenspiel, *Engineering Flow and Heat Exchange*, Springer, New York **2014**.

[5]   O. Levenspiel, *Chem. Eng. Sci.* **1983**, *38*, 2035–2045. DOI: https://doi.org/10.1016/0009-2509(83)80107-9

[6]   W. Bender, N1 *Wärmeübertragung in Regeneratoren*, in *VDI-Wärmeatlas* (Eds: P. Stephan et al.), 12. ed., Springer Vieweg Verlag, Düsseldorf **2019**.

[7]   C. C. Furnas, *Ind. Eng. Chem.* **1930**, *22*, 26–31, 721–731. DOI: https://doi.org/10.1021/ie50247a008

[8]   H. Hausen, *Z. Angew. Math. Mech.* **1929**, *9*, 173–200. DOI: https://doi.org/10.1002/zamm.19290090302

[9]   A. Uniyal, A. Sharma, *Int. J. Appl. Eng. Res.* **2018**, *13*, 42–48.

[10] M. Hänchen, S. Brückner, A. Steinfeld, *Appl. Therm. Eng.* **2011**, *31*, 1798–1806. DOI: https://doi.org/10.1016/j.applthermaleng.2010.10.034

[11] P. Klein, T. H. Roos, T. J. Sheer, *Energy Procedia* **2014**, *49*, 840–849. DOI: https://doi.org/10.1016/j.egypro.2014.03.091

[12] *Chemical Technology: From Principles to Processes*, 2. ed. (Eds: A. Jess, P. Wasserscheid), Wiley-VCH, Weinheim **2020**.

[13] *Technische Chemie* (Eds: M. Baerns, A. Behr, A. Brehm, J. Gmehling, H. Hofmann, U. Onken, A. Renken), Wiley-VCH Verlag GmbH, Weinheim **2006**.

[14] *Grundoperationen. Lehrbuch der Technischen Chemie Band II* (Eds: J. Gmehling, A. Brehm), Georg Thieme Verlag, Stuttgart **1996**.

[15] W. Kast, *Adsorption aus der Gasphase*, VCH-Verlagsgesellschaft, Weinheim **1988**.

[16] D. M. Ruthven, *Encyclopedia of Separation Technology*, Wiley-Interscience, New York **1997**.

[17] D. M. Ruthven, *Principles of Adsorption and Adsorption Processes*, Wiley, New York **1984**.

[18] K. Sattler, *Thermische Trennverfahren: Grundlagen, Auslegung, Apparate*, Wiley-VCH, Weinheim **2001**.

[19] W. Kast, *Chem. Ing. Tech.* **1981**, *53*, 160–172. DOI: https://doi.org/10.1002/cite.330530304

[20] W. Kast, W. Otten, *Chem. Ing. Tech.* **1987**, *59*, 1–11. DOI: https://doi.org/10.1002/cite.330590103

[21] R. C. Brown, *Int. J. Occup. Saf. Ergon.* **1995**, *1*, 330–373. DOI: https://doi.org/10.1080/10803548.1995.11076330

[22] G. Grevillot, S. Marsteau, C. Vallieres, *J. Occup. Environ. Hygiene* **2011**, *6*, 279–288. DOI: https://doi.org/10.1080/15459624.2011.567131

[23] D. M. Ruthven, *AIChE J.* **1978**, *24*, 540–542. DOI: https://doi.org/10.1002/aic.690240323

[24] D. R. Garg, D. M. Ruthven, *AIChE J.* **1975**, *21*, 200–202. DOI: https://doi.org/10.1002/aic.690210137

[25] E. Glueckauf, *Trans. Faraday Soc.* **1955**, *51*, 1540–1551. DOI: https://doi.org/10.1039/TF9555101540

[26] K. S. Hwang, W. K. Lee, *Sep. Sci. Technol.* **1994**, *29*, 1857–1891. DOI: https://doi.org/10.1080/01496399408002177

[27] M. Polakovic, T. Gorner, F. Villieras, P. de Donato, J. L. Bersillon, *Langmuir* **2005**, *21*, 2988–2996. DOI: https://doi.org/10.1021/la047143+

[28] C. Kern, *Ph. D. Thesis*, Technical University Aachen **2003**.

[29] C. Kern, A. Jess, *Chem. Eng. Sci.* **2005**, *60*, 4249–4264. DOI: https://doi.org/10.1016/j.ces.2005.01.024

[30] D. Tang, C. Kern, A. Jess, *Appl. Catal., A* **2004**, *272*, 187–199. DOI: https://doi.org/10.1016/j.apcata.2004.05.040